Induction of enhanced magnetic behavior in gold, silver, and copper by doping with $SrFe_{12}O_{19}$ nanoparticles

Noam Ralbag,[1,3] Israel Felner,[2,3,*] and David Avnir[1,3,†]
[1]*Institute of Chemistry, The Hebrew University of Jerusalem, Jerusalem 9190401, Israel*
[2]*Racah Institute of Physics, The Hebrew University of Jerusalem, Jerusalem 9190401, Israel*
[3]*Center for Nanoscience and Nanotechnology, The Hebrew University of Jerusalem, Jerusalem 9190401, Israel*

(Received 4 November 2018; revised manuscript received 15 January 2019; published 12 February 2019)

Enhanced magnetic moment is induced in nonmagnetic metals. Specifically, gold, silver, and copper are rendered with bulk magnetic behavior by doping these metals with ferrimagnetic strontium hexa-ferrite ($SrFe_{12}O_{19}$) nanoparticles. The doped metals exhibit classical macroscopic permanent magnetic properties. Remarkably, detailed magnetization studies reveal that the saturation moments (M_S) of these materials are enhanced by a factor of 5–8 compared to pure $SrFe_{12}O_{19}$ nanoparticles. The enhancement order is Cu > Ag > Au. A mechanism is suggested for the enhancement and for its order, based on a full materials characterization of these $SrFe_{12}O_{19}$@Metals.

DOI: 10.1103/PhysRevB.99.064411

I. INTRODUCTION

We report the induction of apparent magnetic behavior in the coinage metals: gold, silver, and copper. Entrapment of ferrimagnetic strontium hexaferrite ($SrFe_{12}O_{19}$, SFO) nanoparticles (NPs) within these metals renders these classically nonmagnetic metals with apparent magnetic behavior. Furthermore, a large enhancement in the magnetic moments of the resulting SFO@metals compared with pure SFO is obtained.

Inducing in metals properties which are not their classical ones is a key challenge in materials science, as such inductions open the route to new functional metallic materials. Molecular doping of metals [1,2] is a materials methodology which was developed in recent years and has enabled that challenge. For instance, entrapment of organometallic catalysts within metallic catalysts led to multifunctional composites which exhibited multistep catalytic capabilities [3]; entrapment of antibacterial agents in silver—which is an antibacterial metal—led to a synergistic superkiller of pathogenic bacteria [4]; entrapment of polydimethylsiloxane in iron led to the reduction of its corrosion rate to 3 μm per year [5]; doped Cu-Pt alloy led to dual electrochemical activity [6]; the use of doped silver electrodes led to a type of battery based on such electrodes [7]; and more [8–11].

The challenge we set up to solve in this paper is to entail magnetic behavior in metals which are good conductors but not magnetic. The idea is to go beyond the magnetic iron, cobalt, and nickel metals and to open that property to practically any selected metal from the periodic table, by proper doping. As for the metals, we have selected in this paper the nonmagnetic coinage metals gold, silver, and copper; as for the magnetism inducing dopant, we selected nanoparticles (60 nm) of SFO, a ferrimagnetic material (Curie temperature $T_M = 750$ K) widely used in many industrial and commercial applications.

The synthesis of NP-metal composites, enabled by dispersing the NPs in the molten metal, is known especially for metal reinforcement applications [12,13]. Here we report the development of the protocol of doping a metal with nanoparticles using solution chemistry.

The common use of SFO is due to its moderate saturation magnetization (M_S), high coercive field (H_C), low cost, and chemical stability. Let us recall some of its crystallographic and magnetic properties, relevant for this report. $SrFe_{12}O_{19}$ crystallizes in a hexagonal structure ($P6_3/mmc$), where each unit cell contains two SFO formula units and 64 atoms. The 24 high spin Fe^{3+} ($3d^5$) ions ($S = 5/2$) distribute over five distinct symmetry sites: three octahedral sites ($2a$, $4f_2$, and $12k$), one tetrahedral site ($4f_1$), and one trigonal bipyramidal fivefold coordination ($2b$) site. These five Fe sites are magnetically coupled via superexchange interactions through the oxygen ions. Sixteen Fe^{3+} ions which reside in the $4f_2$ and $12k$ sites have the same magnetic spin configuration (up) opposite to eight Fe^{3+} ions which occupy the three other sites $2a$, $2b$, and $4f_1$ (down) [14–17]. For an ideal occupation each high spin Fe^{3+} ion has a magnetic moment of 5 μ_B, and therefore the net moment is 40 μ_B per unit cell or 20 μ_B/f.u. [14]. Indeed, the extrapolated saturation magnetization at zero temperature $M_S(0)$, is 19.7 μ_B/f.u. [18]. This value corresponds to 515 emu mL^{-1} or to 102 emu g^{-1}. The temperature dependence of M_S was measured and calculated by taking into account the exchange integrals for all five Fe^{3+} sites, and the deduced M_S value at room temperature (RT) was found to be 74.3 emu g^{-1} [14,18]. The coercive field (H_C) of SFO at RT is affected by the annealing times and/or by the annealing temperatures. For short annealing time of materials synthesized by sol-gel autocombustion method at 800 or 900 °C, H_C remains small (300–700 Oe) and almost constant. Above a critical heat-treatment time, H_C increases up to 3500 Oe [19].

*Israel.felner@mail.huji.ac.il
†David.Avnir@mail.huji.ac.il

This increase is explained by the increase of the particle size to the normal state of the single domain NPs. For much longer times, H_C decreases due to grains growth and the appearance of domain walls. For a single domain, the large H_C is due to the rotation of the magnetization with the applied field, whereas for multidomain structure the smaller H_C takes place through the displacement of the domain walls. NPs which were annealed at various temperatures also show a significant change in their H_C values [20].

The details of conversion of gold, silver, and copper into functional metallic magnets, the large enhancement effect—up to a factor of 8 compared with pure SFO NP M_S, and extensive dc magnetic studies are detailed next. This unique magnetization enhancement is reproducible and has been observed for all three coinage metals, following an enhancement order of Cu > Ag > Au. A tentative interpretation for the enhancement and for this order is provided in the Discussion section.

II. EXPERIMENTAL DETAILS

The synthesis procedures for all SFO@metals are described in detail in the Supplemental Material [21]. The morphology and the structural characteristics of the powders were studied by high-resolution scanning electron microscopy (HR-SEM) with a FEI Sirion instrument fitted with an energy dispersive spectroscopy (EDS) free detector. Specific surface areas were calculated from nitrogen adsorption/desorption isotherms obtained with a Micromeritics ASAP 2020 surface area analyzer. Density measurements were performed using a Micromeritics Accupyc 1340 pycnometer. Powder x-ray-diffraction (XRD) measurements were carried out using a Philips diffractometer [CuKα1 (1.5406 Å) with a step scan mode 0.02 s^{-1}]. The temperature dependence $M(T)$ of the magnetization and the isothermal $M(H)$ magnetization at various temperatures were measured using commercial (Quantum Design) superconducting quantum interference device magnetometers. In order to confirm the obtained results and to exclude instrumental effects the $M(H)$ plots were measured in two different magnetometers.

III. RESULTS AND DISCUSSION

A. Magnetic properties studies

1. Doped copper, silver, and gold as classical permanent magnets

We begin with the macroscopic observations in which gold, silver, and copper disks behave as classical permanent magnets. Figure 1(a) shows a disc of doped silver (7.98-wt.-% SFO) which was magnetized by a dc permanent magnet of ~4 kG: Iron powder sprinkled around the disc clearly follows the classic magnetic field lines. Figure 1(b) shows the magnetic attraction of the doped gold, silver, and copper (without being magnetized) either as powders or as discs to an external magnet.

In the next sections we study in detail these magnetic properties, revealing not only that we have obtained coin metals which behave as magnets but that their saturated magnetic moments (M_S) are significantly enhanced. For the sake of clarity we describe first the magnetic characterization

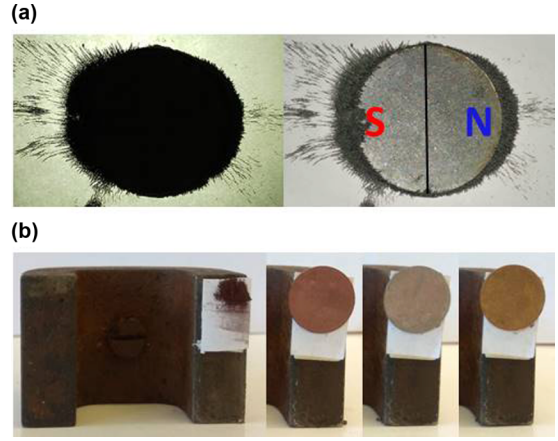

FIG. 1. Magnetic behavior of the coinage metals. (a) A silver magnet. Iron powder sprinkled around the SFO doped coin (d = 13 mm) follows the magnetic force field lines. Top and bottom illumination is shown. (b) The attraction of the doped coinage metals to a magnet. Left: Copper powder. Right: Discs of (from left to right) copper, silver, and gold.

of the commercial pure SFO NPs—this will serve as a comparative background for the magnetic characterization of the doped SFO@metals, which will be described next. Later on we provide a detailed materials characterization study of these doped metals, and these characterizations will serve for the proposed interpretation of the correlation between the materials properties and the magnetic behavior.

2. Magnetization measurements of SFO NPs

The isothermal magnetization [$M(H)$] plots of the ferrimagnetic SFO NPs (average particle size d = 60 nm) were measured at various temperatures and the resulting curves measured at 295 K are shown in Fig. 2(a). The typical $M(H)$ plot increases sharply up to ~20 kOe and then linearly up to 50 kOe. This curve can be fitted to $M(H) = M_S + \chi_p H$, where M_S is the saturation magnetization, and $\chi_p = 6.5 \times 10^{-5}$ emu g^{-1} is the linear intrinsic paramagnetic susceptibility. The deduced $M_S = 65.6 \pm 0.2$ emu g^{-1} is attributed to the SFO NPs, which are magnetically ordered at RT, well below T_M. It is well known that T_M of SFO NPs increases with the reduction of particle size, and for particles with an average size of 20 nm T_M = 750 K [17]. The same T_M was also observed for bulk material [14], thus we may assume this value as T_M of the pure SFO NPs. The obtained M_S is lower (by ~11%) than 74.3 emu g^{-1} measured for bulk SFO [18], or 70−72 emu g^{-1} for platelike-shaped particles having similar dimensions [22]. This reduction is well expected because for NPs the surface, which contributes significantly to M_S, may be affected by structural imperfections that cause spin canting [23]. Alternatively, the linear $\chi_p H$ may stem from a tiny fraction of paramagnetic SFO NPs for which the T_M values are lower than RT.

Similar $M(H)$ plots were measured at lower temperatures, and the same treatment yields M_S = 95.8(2), 88.8(2), and 79.2(2) emu g^{-1} for T = 5, 100, and 200 K, respectively. Note that M_S at 5 K is only 6% lower than the value of $M_S(0)$ = 102 emu g^{-1}, cited above [18]. It is well accepted

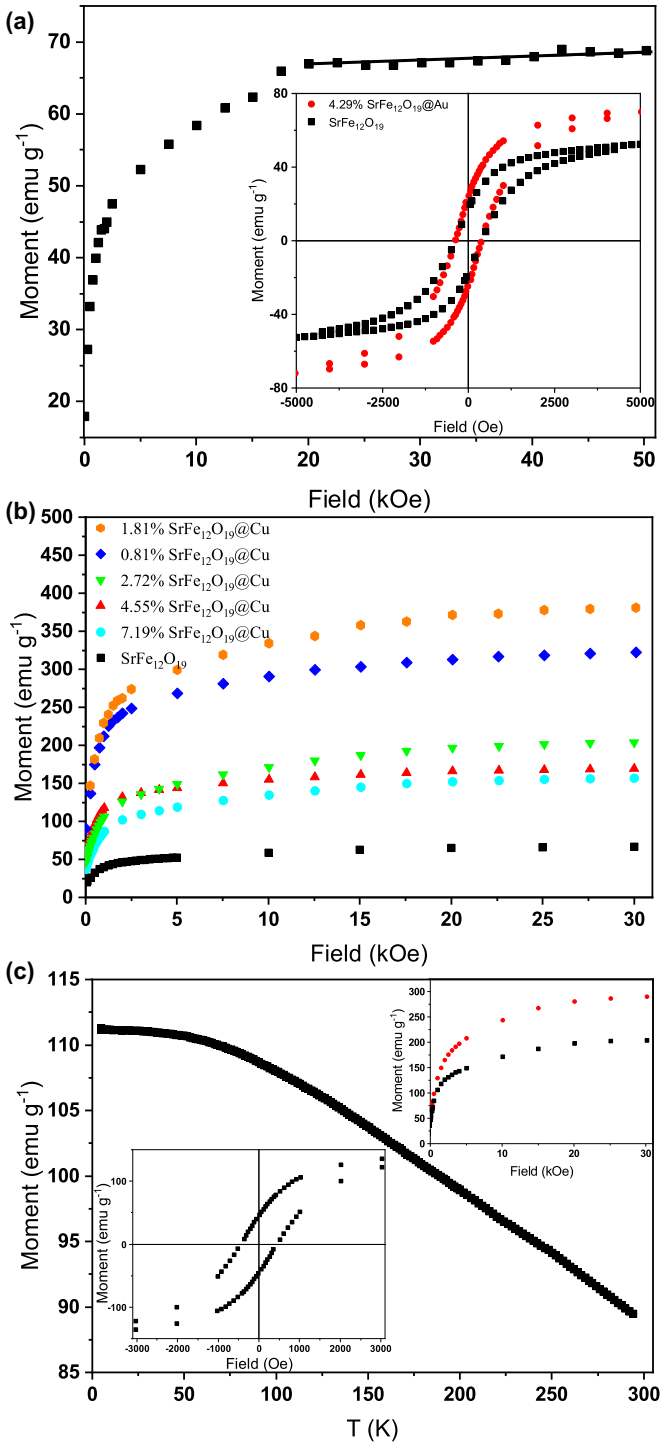

FIG. 2. Magnetization measurements of SFO NPs and SFO@Cu. (a) Isothermal magnetization of SFO NPs (average particle size 60 nm) measured at 295 K. The inset shows the RT hysteresis loops of SFO (black squares) and of 4.29-wt.-% SFO@Au (red circles; the red lines are to guide the eyes). (b) Isothermal magnetization plots measured at 295 K of SFO@Cu at various dopant NPs concentrations; note the high magnetization saturation values at the lower concentrations. See also Fig. 3. (c) The zero-field cooled plot of 2.72-wt.-% SFO@Cu, measured at 1 kOe. The upper inset shows two $M(H)$ curves measured at 5 (red circles) and 295 K (black squares) and the lower inset presents the RT hysteresis loop. All weight normalizations are to SFO.

that for a single domain structure the average particle size is proportional to its magnetic ordering temperature and to its magnetocrystalline anisotropy and inversely proportional to its M_S. For SFO NPs, the critical particle size value between single domain and multidomain is around 650 nm [24]. That definitely means that our pure SFO material is made of single-domain particles.

The $M(H)$ loop at 295 K displays a hysteresis loop with a coercive field $H_C = 420(10)$ Oe, as shown in Fig. 2(a) (inset, black squares). Due to the high T_M of the SFO NPs, H_C does not change much with the temperature and at 5 K we measured $H_C = 450(10)$. These H_C values are much smaller than H_C of bulk materials [18,20], but are in a reasonable agreement with values reported in Ref. [19].

3. *Cu, Ag, and Au doped with SFO NPs: Enhanced magnetization moments*

The RT isothermal magnetization of selected concentrations of SFO NPs entrapped in Cu is shown in Fig. 2(b) and compared with pure SFO. Large increases in the SFO (SFO weight-normalized) saturation magnetic moment values compared to pure SFO are clearly evident. The effect is particularly strong for the lower concentrations, exceeding by a factor of 4–5 $M_S = 65.6(2)$ emu g^{-1} obtained for the pure SFO powder; e.g., for 1.81 and 0.81% SFO@Cu, $M_S = 328(10)$ and 271(10) emu g^{-1}, respectively. At higher concentrations, lower M_S values are observed, e.g., for 7.19% $M_S = 155$ emu g^{-1}. Below, we propose an interpretation to this concentration effect.

A zero-field cooled curve (measured at 1 kOe) of 2.72-wt.-% SFO@Cu is plotted in the main frame of Fig. 2(c). It is readily observed that $M(T)$ is almost constant up to 55 K and then gradually decreases (by ~20%) down to RT. Similar typical curves were observed for other samples described hereafter. This behavior is consistent with the density functional theory calculated $M(T)$ for SFO, based on its magnetic structure, in which the 12 Fe^{3+} ions reside in five different sites as described above [18]. Figure 2(c) also shows the $M(H)$ curves at 5 and 295 K ($M_S = 292$ and 206 emu g^{-1}, respectively—upper inset) and the hysteresis loop measured at 295 K, where $H_C = 425(5)$ Oe (lower inset) for this material. Although M_S (at RT) is approximately three times higher than that of SFO [Fig. 2(b)] both samples have the same H_C value, indicating clearly that only M_S is enhanced in the SFO doped particles in Cu as well as in Ag and Au [see also Fig. 2(a) inset] for 4.29-wt.-% SFO@Au.

The $M(H)$ plots for SFO doped in Ag and Au are presented in Fig. 3. Here again, M_S of all diluted samples is much higher than that of the pure SFO NPs, e.g., $M_S = 515$ and 304 emu g^{-1} were obtained for 0.25- and 0.98-wt.-% SFO doped in Au [Fig. 3(b)] and Ag [Fig. 3(a)], respectively. Note that M_S obtained for 0.25 wt. % in Au [Fig. 3(b) red dots] is eight times higher than M_S for pure SFO. On the other hand, the higher concentration materials show lower enhancement or similar M_S values compared to pure SFO. In contrast to the random particles distribution in the dilute samples, at high concentrations the SFO particles aggregate into clusters. Thus, the model proposed (below) for the enhanced M_S of the diluted samples does not apply for the higher concentrations.

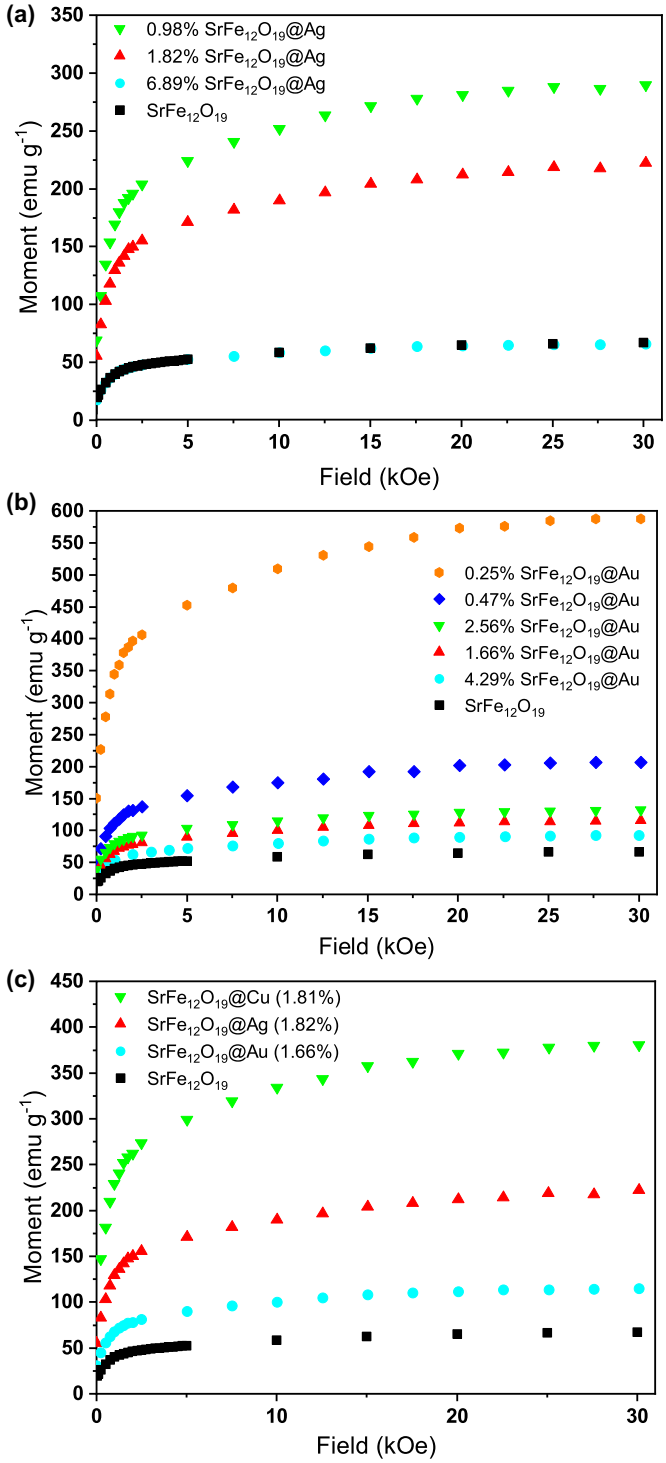

FIG. 3. Magnetization enhancement. Isothermal magnetization plots measured at 295 K of various concentrations of (a) SFO@Ag and (b) SFO@Au. Note again the high M_S values for low concentrations. M_S for 0.25-wt.-% SFO@Au is eight times higher than that of pure SFO. (c) Isothermal magnetization plots for similar concentrations of SFO entrapped in Cu, Ag, and Au. All weight normalizations are to SFO.

Nevertheless, the RT H_C of the concentrated samples is similar to that of SFO [Fig. 2(a) inset].

As a blank test, we also measured the RT $M(H)$ curve of pure Au particles (without SFO as dopant), which followed the same chemical procedure as described in the Supplemental Material [21]. As expected, a linear diamagnetic plot (not shown) with a slope of -2.61×10^{-7} was obtained and the moment value obtained at 50 kOe ($-0.012\,\mathrm{emu\,g^{-1}}$) is five orders of magnitude lower than M_S obtained for SFO doped materials. That means that the pure Au contribution to SFO@Au can be neglected.

In order to compare between the three coinage metal matrices, we present in Fig. 3(c) three similar compositions (with an uncertainty of 10%) which definitely indicate that the enhancement order is Cu > Ag > Au. In the discussion we shall offer an interpretation to this order of enhancement.

B. Metal doping methodology and structural characterization

In this section we describe the synthetic method of metal doping with SFO nanoparticles and the structure of the resulting materials—these will be used in the next section to provide a proposed interpretation to the magnetization observations detailed above.

In general, the challenge of entrapping NPs requires a route which is devoid of stabilizers, which are routinely used for preparation of homogeneous sols, so that the entrapped NP will be without a shell of molecules that separate them from direct contact with the metal. None of the several methods of reductive entrapment we developed in recent years [1,2] was found suitable for this purpose, thus a further method had to be developed. After scanning of several alternative metal cation reduction procedures without NP stabilizers, we found that metal reduction in polyols at elevated temperature keeps the NP dispersed (Fig. 4). The procedure (see Experimental Details) works well not only for SFO NPs but also for other types of NPs as well (to be reported separately). Specifically, the polyol as a reaction solvent is an easily washable NP dispersant and reducing agent at the same time. As an example, the reactions for SFO@Cu are as follows.

Formation of the reducing acetaldehyde:

$$\mathrm{CH_2OH - CH_2OH} \xrightarrow{\mathrm{NaOH}} \mathrm{CH_3CHO + H_2O} \qquad (1)$$

Reduction of the metal ions in the presence of the dopant SFO NPs:

$$2\mathrm{CH_3CHO} + \mathrm{Cu^{2+}} + 2\mathrm{OH^-} + \mathrm{dopant} \longrightarrow \mathrm{dopant@Cu} + \mathrm{CH_3COCOCH_3} + 2\mathrm{H_2O}. \qquad (2)$$

Similar reactions for SFO@Ag and SFO@Au are listed in the Supplemental Material [21].

The morphology of the composites [see Fig. 4(a) and Fig. S1 in the Supplemental Material [21]] is made of aggregated metallic nanocrystallites where the SFO NPs are physically entrapped in the interstitial porosity. NPs are clearly seen in the figure. Elemental mapping performed by EDS which traces Fe [Fig. 4(b)] confirms the random distribution of the SFO NPs. The XRD pattern of the composites (see Fig. S2 in the Supplemental Material [21]) is characteristic of the corresponding metal and the ferrite. Applying Scherrer's equation to the metals' reflections of the XRD patterns indicates that

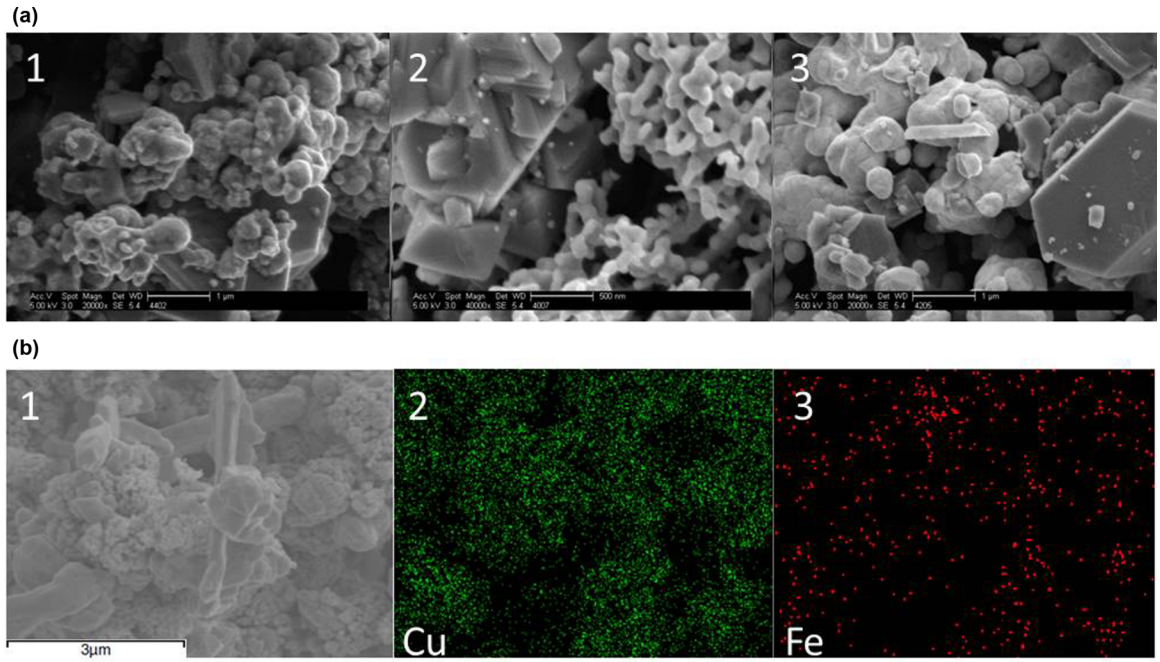

FIG. 4. Material characterizations of the doped metals. (a) HR-SEM images. 1: 0.80-wt.-% SFO@Cu (scale bar = 1 μm). 2: 0.98-wt.-% SFO@Ag (scale bar = 500 nm). 3: 1.66-wt.-% SFO@Au (scale bar = 1 μm). (b) EDS elemental mapping of SFO@Cu (4.55 wt. %). 1: SEM image. 2 and 3: The corresponding Cu and Fe maps.

the particles sizes are 47, 52, and 39 nm for Cu, Ag, and Au, respectively.

IV. FURTHER DISCUSSION

We have described a method of inducing apparent magnetization in metals which are devoid of this property, by doping with SFO NPs. The three coinage metals—Cu, Ag, and Au—were the focus of this paper. All SFO doped materials have similar H_C values to that of pure SFO NPs (∼420 Oe at RT)**.** A very interesting enhancement of the M_S—up to a factor of 8—is observed for all low concentrations (e.g., 0.25 wt. %) of SFO@metals. For the higher dopant concentrations (∼7−8%) the M_S obtained are closer to that of the pure SFO NPs ferrite. At first glance, one would expect the opposite, that is, an enhancement of the effect as more of the dopant is contained in the metal, but in fact that observation points to a conclusion that the enhancement requires intimate contact between SFO NPs and the coinage metallic surface which cages it; as can be seen in Fig. S1a in the Supplemental Material [21], high concentrations result in the entrapment of NP aggregates so that the immediate neighbors of an average ferrite NP are other ferrite NPs, leading to smaller M_S. What then is (i) the possible origin of that enhancement and (ii) its order of Cu > Ag > Au?

Enhancements of magnetic properties in multilayered heterostructures and due to placement of a magnetic material in contact with a metal or to a metal-based compound have already been observed [25]. They were interpreted in terms of spin-orbit coupling and in terms of ferromagnetic instability [25]. Examples include (i) multilayered structures such as MgO/Fe/MgO trilayers [26] and Co/Pd bilayers, in which the magnetic enhancement occurs at the interface between the magnetic and metallic monolayers [27]; (ii) magnetic nickel NPs embedded in multiwalled carbon nanotubes (MWCNTs), in which it was proposed that the moment enhancement arises from the interplay between Ni NPs and the strong diamagnetic nature of the MWCNT [28]; (iii) γ-Fe_2O_3 core-Cu shell particles [29], where it was proposed that the enhancement is caused by Cu-O-Fe interactions [30]; and (iv) Fe_3O_4 core-Au shell particles, where again interfacial interactions between the magnetic core and the metallic shell were proposed [31], namely, that the enhancement is accounted for by spin polarization of the metal atoms. The penetration depth of this polarization is low—1–2 nm—and therefore a significant total enhancement is observed only when there is a large contact interface. None of these observations are relevant to our systems. Furthermore, ferromagnetic hysteresis loops at RT (H_C = 250 Oe) were measured in a polarized strong interacting thiol capped by Au NPs [32]. It was found that the Au atoms exhibit a distinct magnetic moment of $0.036\mu_B$ (∼1 emu/g). It was proposed that the thiol ligand induces extra localized holes in the 5*d* Au band, which lead to the observed magnetic moment. On the other hand, Au NPs dispersed by nonreactive media are diamagnetic, similar to that of bulk Au [33]. Similar results propose that only the NP surface of coinage atoms is magnetic, and that the interior atoms remain diamagnetic [33]. We may assume that the ferrimagnetic SFO NPs also induce a similar magnetic moment in the coinage metal bands. However, this procedure induces a very small moment and cannot account for the two- to eightfold enhanced M_S exhibited in Figs. 2 and 3.

To date, an enhanced magnetic moment was observed in one sample of iron oxide (Fe_3O_4) NPs coated with Au [31], and the model proposed there seems to be more appropriate to our case. Qualitatively, we propose that similar interfacial

interpretation is relevant for our case, namely, that the SFO affects the spin polarization of the metal in contact. We propose the existence of a contact potential and a radial electric field at the SFO coinage metal (M) interfaces (perpendicular to the interface): $E = -(dV/dr)_{r=\lambda}$ where λ is the radius of the interface. This electric field induces a Rashba-type spin-orbit interaction given by $H = -\alpha(h/2\pi)^2 LzSz$ where α is the spin-orbit coupling strength which is strongly proportional to the contact potential and depends on the contact cross section [31]. The chemical potential gradient between the two components at the interface is enough to capture conduction electrons from the metals and to induce a large orbital moment at the surface. More specifically, the enhanced M_S is argued to stem from free metallic electrons at the surfaces and that is the largest enhancement obtained for copper. Two other (less preferable) hypotheses as to the possible origin of this enhancement are summarized in the Supplemental Material [21].

Supporting this view is the observation that the M_S enhancement is largest for copper and smallest for gold (Cu > Ag > Au), as this is also the order of the metals' average experimental electric polarizability [34] values, which are 56.7, 54.5, and 44.1 atomic units for Cu, Ag, and Au, respectively [35]. This property of the metals is relevant because the electric polarizability reflects the response of the charge distribution in an atom caused by any external filed, such as induced by the SFO NPs. The extended explanation is discussed in the Supplemental Material [21].

Finally, we recall that composites of magnetite—Fe_3O_4 [36]—in various hosts have been widely investigated [37–41] due to a range of applications which include catalysis [39,42], biomedicine [40], and imaging [37]. We believe that the magnetic NP@metals reported here will find their applications in these areas as well, and in applications which require conductivity and magnetism in the same material.

ACKNOWLEDGMENTS

This work was supported by the Ministry of Science, Technology, and Space, Israel, Grants No. 2015-6-161 and No. 2016-3-12948, and by the Israel Science Foundation Grant No. 703/12. We thank Dr. Vladimir Uvarov of the Center for Nanoscience and Nanotechnology, The Hebrew University, for analytical support.

[1] D. Avnir, Acc. Chem. Res. **47**, 579 (2014).
[2] D. Avnir, Adv. Mater. 1706804 (2018).
[3] L. Shapiro, M. Driess, and D. Avnir, Chem. Cat. Chem. **7**, 2033 (2015).
[4] R. Ben-Knaz, R. Pedahzur, and D. Avnir, RSC Adv. **3**, 8009 (2013).
[5] Y. Aouat, G. Marom, and D. Avnir, Eur. J. Inorg. Chem. **2016**, 1488 (2016).
[6] H.-P. Yang, Y.-N. Yue, S. Qin, H. Wang, and J.-X. Lu, Green Chem. **18**, 3216 (2016).
[7] O. Sinai and D. Avnir, Chem. Mater. **23**, 3289 (2011).
[8] I. Yosef and D. Avnir, Chem. Mater. **18**, 5890 (2006).
[9] H. Behar-Levy and D. Avnir, Chem. Mater. **14**, 1736 (2002).
[10] H.-P. Yang, S. Qin, H. Wang, and J.-X. Lu, Green Chem. **17**, 5144 (2015).
[11] H.-P. Yang, Q. Fen, H. Wang, and J.-X. Lu, Electrochem. Commun. **71**, 38 (2016).
[12] K. M. Sree Manu, S. Arun Kumar, T. P. D. Rajan, M. Riyas Mohammed, and B. C. Pai, J. Alloys Compd. **712**, 394 (2017).
[13] S. M. Hong, E. K. Park, J. J. Park, M. K. Lee, and J. Gu Lee, Mater. Sci. Eng. A **643**, 37 (2015).
[14] B. T. Shirk and W. R. Buessem, J. Appl. Phys. **40**, 1294 (1969).
[15] A. E. Ramírez, N. J. Solarte, L. H. Singh, J. A. H. Coaquira, and S. Gaona, J. Magn. Magn. Mater. **438**, 100 (2017).
[16] M. Cernea, S.-G. Sandu, C. Galassi, R. Radu, and V. Kuncser, J. Alloys Compd. **561**, 121 (2013).
[17] A. Vijayalakshmi and N. S. Gajbhiye, J. Appl. Phys. **83**, 400 (1998).
[18] J. Park, Y.-K. Hong, S.-G. Kim, S. Kim, L. S. I. Liyanage, J. Lee, W. Lee, G. S. Abo, K.-H. Hur, and S.-Y. An, J. Magn. Magn. Mater. **355**, 1 (2014).
[19] N. Rezlescu, C. Doroftei, E. Rezlescu, and P. D. Popa, J. Alloys Compd. **451**, 492 (2008).
[20] N. Kumar, A. Kumar, R. Jha, A. Dogra, R. Pasricha, R. K. Kotnala, H. Kishan, and V. P. S. Awana, J. Supercond. Nov. Magn. **23**, 423 (2010).
[21] See Supplemental Material at http://link.aps.org/supplemental/10.1103/PhysRevB.99.064411 for experimental details, reactions of the formation of SFO Ag and SFO Au, additional materials characterization including Figs. S1 and S2 and Tables S1 and S2, alternative (less likely) interpretations of the magnetization enhancement, more on the order of the magnetic enhancement for the coinage metals, and Refs. [S1–S3].
[22] N. A. Sapoletova, S. E. Kushnir, Y. Hui Li, S. Yong An, J. Seo, and K. Heon Hur, J. Magn. Magn. Mater. **389**, 101 (2015).
[23] P. Zhang and T. K. Sham, Phys. Rev. Lett. **90**, 245502 (2003).
[24] Z. F. Zi, Y. P. Sun, X. B. Zhu, Z. R. Yang, J. M. Dai, and W. H. Song, J. Magn. Magn. Mater. **320**, 2746 (2008).
[25] F. Hellman, A. Hoffmann, Y. Tserkovnyak, G. S. D. Beach, E. E. Fullerton, C. Leighton, A. H. MacDonald, D. C. Ralph, D. A. Arena, H. A. Dürr, P. Fischer, J. Grollier, J. P. Heremans, T. Jungwirth, A. V. Kimel, B. Koopmans, I. N. Krivorotov, S. J. May, A. K. Petford-Long, J. M. Rondinelli, N. Samarth, I. K. Schuller, A. N. Slavin, M. D. Stiles, O. Tchernyshyov, A. Thiaville, and B. L. Zink, Rev. Mod. Phys. **89**, 025006 (2017).
[26] E. Jal, J. B. Kortright, T. Chase, T. Liu, A. X. Gray, P. Shafer, E. Arenholz, P. Xu, J. Jeong, M. G. Samant, S. S. P. Parkin, and H. A. Dürr, Appl. Phys. Lett. **107**, 092404 (2015).
[27] S. C. Hong, T. H. Rho, and I. Jae, J. Magn. Magn. Mater. **140**, 697 (1995).
[28] J. Wang, P. Beeli, Y. Ren, and G.-m. Zhao, Phys. Rev. B **82**, 193410 (2010).
[29] R. D. Desautels, E. Skoropata, Y. Y. Chen, H. Ouyang, J. W. Freeland, and J. Van Lierop, Appl. Phys. Lett. **99**, 262501 (2011).

[30] R. D. Desautels, E. Skoropata, Y.-Y. Chen, H. Ouyang, J. W. Freeland, and J. van Lierop, J. Phys. Condens. Matter **24**, 146001 (2012).
[31] S. Banerjee, S. O. Raja, M. Sardar, N. Gayathri, B. Ghosh, and A. Dasgupta, J. Appl. Phys. **109**, 123902 (2011).
[32] P. Crespo, R. Litrán, T. C. Rojas, M. Multigner, J. M. de la Fuente, J. C. Sánchez-López, M. A. García, A. Hernando, S. Penadés, and A. Fernández, Phys. Rev. Lett. **93**, 087204 (2004).
[33] A. Hernando, P. Crespo, and M. A. García, Phys. Rev. Lett. **96**, 057206 (2006).
[34] L. Ma, J. Indergaard, B. Zhang, I. Larkin, R. Moro, and W. A. de Heer, Phys. Rev. A **91**, 010501(R) (2015).
[35] P. Schwerdtfeger and J. K. Nagle, Mol. Phys. 1 (2018), doi: 10.1080/00268976.2018.1535143.
[36] H. Yu, M. Chen, P. M. Rice, S. X. Wang, A. R. L. White, and S. Sun, NANO Lett. **5**, 379 (2005).
[37] H. Rui, R. Xing, Z. Xu, Y. Hou, S. Goo, and S. Sun, Adv. Mater. **22**, 2729 (2010).
[38] J. Gao, H. Gu, and B. Xu, Acc. Chem. Res. **42**, 1097 (2009).
[39] L. Jing, Y. Xu, S. Huang, M. Xie, M. He, H. Xu, H. Li, and Q. Zhang, Appl. Catal. B Environ. **199**, 11 (2016).
[40] H. Gu, Z. Yang, J. Gao, A. C. K. Chang, and B. Xu, J. Am. Chem. Soc. **127**, 34 (2004).
[41] S. Peng and S. Sun, Angew. Chemie Int. Ed. **46**, 4155 (2007).
[42] L. Ai, C. Zeng, and Q. Wang, Catal. Commun. **14**, 68 (2011).